


Research Article

Uncertainty-Based Capacity Factors of Operational Wind Turbines Using the Generalized Likelihood Uncertainty Estimation (GLUE) Method

Tsang-Jung Chang,^{1,2,3} Kao-Hua Chang,⁴ Hsiang-Lin Yu ,^{1,2} Chung-Yi Chen,¹ and Shu-Yuan Pan¹

¹Department of Bioenvironmental Systems Engineering, National Taiwan University, Taipei 106, Taiwan

²Hydrotech Research Institute, National Taiwan University, Taipei 106, Taiwan

³Center for Weather and Climate Disaster Research, National Taiwan University, Taipei 106, Taiwan

⁴Department of Soil and Water Conservation, National Chung-Hsing University, Taichung 402, Taiwan

Correspondence should be addressed to Hsiang-Lin Yu; andy780421@gmail.com

Received 4 September 2023; Revised 29 December 2023; Accepted 18 January 2024; Published 20 February 2024

Academic Editor: Ayman Al-Quraan

Copyright © 2024 Tsang-Jung Chang et al. This is an open access article distributed under the Creative Commons Attribution License, which permits unrestricted use, distribution, and reproduction in any medium, provided the original work is properly cited.

This study proposes a novel framework that couples the general likelihood uncertainty estimation (GLUE) method with a deterministic forecasting approach to conduct a new uncertainty analysis approach for assessing the energy production of operational wind turbines installed in the Jhongtun wind farm at Penghu (an island in the middle of Taiwan Strait). The 10-year measured data of wind speeds and energy output collected on these wind turbines is divided into two 5-year data sets for the present analysis framework of execution and validation to demonstrate the predictability of the GLUE method. The present study considers 15 scenario testing cases with various time periods, *i.e.*, twelve months, the strong-wind (October-March) regime, the weak-wind (April-September) regime, and one year, for the framework to investigate the applicability of the GLUE method on long-term wind energy forecasting. In the execution framework, the 5-year measured data is used by the GLUE method to access the uncertainties involved in the deterministic approach (*i.e.*, the shape and scale parameters of the Weibull wind speed distribution (WWSD), the performance curve, and the capacity factor) with two confidence intervals of 50% and 90%. The framework is then validated by the measured capacity factors in the last 5-year data and compared with the results of the uncertainty analysis approach by the Monte Carlo (MC) approach to discover the applicability of the new uncertainty analysis approach. From the simulated results, it is found that the proposed uncertainty analysis approach provides predictions of confidence intervals that match the measured data better than the MC-based uncertainty analysis approach. Specifically, the proposed approach can match the measured capacity factors in all the simulated scenarios. Conversely, the MC-based approach is found to create narrow confidence intervals that cannot completely capture the measured capacity factors, particularly for the strong-wind, weak-wind, and one-year scenarios. Therefore, this novel uncertainty analysis approach is proven to be useful in predicting the uncertainties of wind energy production.

1. Introduction

Wind energy has been recognized as a promising alternative to nonrenewable energy resources. Furthermore, wind energy is proven to introduce a noteworthy reduction in greenhouse gases (*i.e.*, CO₂) and water consumption, which reveals the effectiveness of wind energy in preserving envi-

ronmental sustainability [1]. So far, the installation of wind turbines and wind farms worldwide has reached a total capacity of 906 GW in 2023 [2]. Such a large amount of energy is harvested from wind turbines installed in the atmospheric boundary layer where the flow is highly turbulent, intermittent, energetic, and unstable, which leads to significant uncertainties in wind energy production. In this

aspect, the integration of wind energy into electricity power systems has a great impact on power system operations, stability, and planning. The most direct way to tackle this problem is to improve the accuracy and reliability of wind energy forecasting. As a result, many studies associated with the investigation of wind energy forecasting techniques have been made in many countries during the past two decades [3–9]. These approaches have been built for various forecasting horizons according to their objectives, *i.e.*, the very short-term forecasting horizon with a time scale from seconds to minutes for wind turbine control, the short-term forecasting horizon with a time scale from hours to days for economic dispatch, the medium-term forecasting horizon with a time scale from days to weeks for maintenance scheduling, and long-term forecasting horizon with a time scale from weeks to months or years for wind power planning, as summarized by Zhang et al. [10].

Summarizing the aforementioned approaches of various wind energy forecasting technologies in the past two decades, as shown in Figure 1, the authors have classified wind energy forecasting approaches into deterministic forecasting and uncertainty analysis based on whether uncertainties are quantified or not. The deterministic forecasting approaches are further divided into two categories: physics-driven forecasting and data-driven forecasting. In the physics-driven forecasting approaches, the physical causes of wind speeds, *i.e.*, pressure and altitude, are considered. These approaches can be then subdivided into wind physics and turbine physics approaches. For the wind physics approaches, the wind speed data can be represented by a probability density function established based on the measured wind speed data. Among various distributions, the Rayleigh or Weibull distributions are often adopted to describe the wind speed distribution. Basically, the Rayleigh distribution is a special case of the Weibull distribution with a constant shape parameter of 2 and a constant location parameter of 0. As the Rayleigh distribution only consists of one parameter (the scale parameter), it is relatively more convenient to use. Nevertheless, the Weibull distribution is more widely used as it has more flexibility from the inclusion of the shape parameter to match the wind speed data. On the other hand, since the fitness of the adopted wind speed probability density function can significantly influence the accuracy of the predicted wind energy, there are various ways to find the optimal parameter set. For example, AI-Quraan et al. [11] developed an artificial intelligence technique with the whale optimization algorithm (WOA) to search for the optimal parameter set and found that the WOA outperforms the maximum likelihood and moment methods. Besides the probability density functions, the wind speed data can be simulated by numerical weather prediction (NWP) models such as the Weather Research and Forecasting (WRF) model. The corresponding wind energy output can be computed in several ways including using the performance curves of wind turbines or from functions that relate the measured wind speed and generated energy output [3, 12, 13]. In terms of the turbine physics approaches, the wind speed is directly given and the corresponding wind energy output under this wind speed is computed based on the

empirical formula from wind tunnel experiments, which is conceptually similar to the use of the standard performance curve of a wind turbine. In contrast to the physics-driven forecasting approaches, the data-driven forecasting approaches, including the stochastic and artificial intelligence (AI) approaches, completely utilize the measured data of wind speeds and energy output to forecast wind energy output through a predictive function [14]. For the stochastic approaches, the predictive function is expressed by probability theory and stochastic processes, *e.g.*, the Kalman filter (KF) by Zuluaga et al. [15] and Bayesian multiple kernel regression by Wang et al. [16]. Nevertheless, the stochastic approaches are found inappropriate for nonlinear data and could lead to significant delays [16]. The AI approaches have recognized robustness and effectiveness in predicting the wind energy output [14], *e.g.*, the artificial neural network (ANN) by Tu et al. [5, 6] and the extreme learning machine (ELM) by Liu et al. [17]. However, the accuracy of wind energy forecasting based on AI approaches significantly relies on the training set. Concerning all the aforementioned deterministic approaches, because of the inevitable uncertainties in the atmosphere that bring natural variations of wind speeds, the predicted wind energy may not match the actual one in some circumstances, *e.g.*, in seasons where the direction or magnitude of winds change frequently [4]. Furthermore, the generated wind energy is found to have nonlinear and no-stable properties which subsequently decrease the predictivity of these approaches.

To resolve the aforementioned difficulties of the deterministic approaches, uncertainty analysis approaches are subsequently proposed based on the aforementioned deterministic forecasting approaches to quantify the uncertainties in the prediction of wind energy [4]. In the uncertainty analysis approaches, a distribution of wind energy is provided instead of a fixed value in the deterministic forecasting approaches. Currently, there are three main categories of uncertainty analysis, *i.e.*, the risk index, scenario, and probabilistic forecasting approaches [10]. For a risk index approach, a risk index is computed to reflect the expected wind energy forecasting error that is directly related to the predictability of wind energy forecasting. Different indexes such as the Meteo-Risk Index (MRI) by Pinson and Kariniotakis [18] and MaxMin/MaxMinMax by Holmgren et al. [19] are proposed for quantifying such a risk. From the viewpoints of the scenario approaches, they consider the spatiotemporal correlation of the uncertainties at different look-ahead time points and geographical positions such that the scenario approaches are suitable for dynamic decision-making problems [20, 21]. For more details on the risk index and scenario approaches, the readers are referred to Zhang et al. [10].

For the probabilistic forecasting approaches in the category of uncertainty analysis, the wind energy output is a probability density function that provides additional information on the quantity of the involved uncertainties. Currently, there are nonparametric and parametric approaches for building the probability density function [10]. Concerning the nonparametric approaches, no assumption is required for describing the distribution shape of any

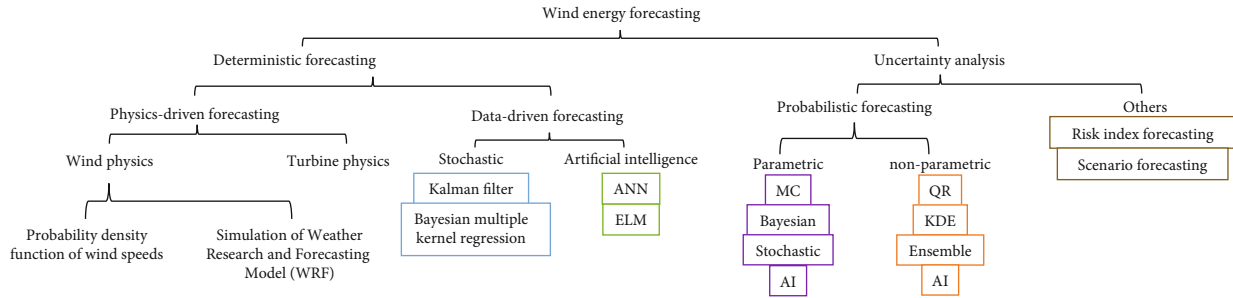


FIGURE 1: The classification of the wind energy forecasting approaches by the present study.

uncertainty such that the nonparametric approaches are distribution-free. Various approaches are built to estimate the wind energy distribution in various ways, such as the quantile regression method (*e.g.*, the Local Quantile Regression (LQR) model by Bremnes [22, 23]), the kernel density estimation (KDE) method (*e.g.*, the KDE method based on copula method by Bessa et al. [24]), the ensemble forecasting method that uses massive WRF ensembles (*e.g.*, the approach that uses the Bayesian Model Averaging (BMA) to average the predicted results of three AI approaches by Wang et al. [25] and the approach by Xie et al. [26] that uses a nonparametric time series forecast model (Infinite Markov Switching Autoregressive, IMSAR) for wind power generation and applies the Bayesian inference with a sampling procedure to quantify the uncertainty based on measured data), and the AI method (*e.g.*, the nonparametric approach by Wan et al. [27]). Although no parameters of the distribution shape are required to be determined, as noted by Zhang et al. [10], the nonparametric approaches are more computationally expensive than the parametric approaches that will be introduced in the next paragraph. Hence, based on the reviews of the deterministic approaches in the second paragraph and the nonparametric approaches in this paragraph, the target of this research is to build a parametric approach based on a physics-driven forecasting approach comprising both the wind and turbine physics approaches.

For the parametric approaches in the category of probabilistic forecasting, the distribution shapes of parameters with uncertainties are analytically defined [10]. Based on the aforementioned objective of the present study (convert a deterministic forecasting approach (physics-driven forecasting approach) to a probabilistic forecasting approach (parametric approach)), as displayed in Figure 2, the authors herein classified various parametric approaches into the MC approaches, GLUE approaches, Bayesian approaches, stochastic approaches, and AI approaches. In the MC approaches, the distributions of uncertain factors are defined, *e.g.*, applying the Weibull distribution for wind speeds, and massive samplings are created to form the resultant wind energy output distribution. For example, Kwon [28] considers the uncertainties in the WWSD (*i.e.*, the shape parameter), ground roughness and performance curve, *etc.*, and uses the MC method to create a huge number of simulated values to evaluate the uncertainties of the wind energy. Mokryani and Siano [29] establish an integrated approach that comprises the MC method and market-

based optimal power flow to evaluate the impact of wind turbine integration into the distribution networks within a market environment. Zhao et al. [30] examine the performance of the probabilistic uncertainty analysis based on the MC method and chaos least squares support vector machine algorithm (Chaos-LS-SVM) for predicting confidence levels of wind energy output. The Bayesian approaches utilize the Bayesian inference method to estimate the parameters of defined distributions of the uncertain factors and then apply the MC method to form the desired distribution, *e.g.*, Bracale and Falco [31] establish an advanced Bayesian approach for short-term wind energy forecasting that includes a mixture of two WWSDs and a Bayesian interface method to find the parameters of the two WWSDs. Then, the MC method is used to find the desired wind energy distribution. Jung et al. [32] propose a Bayesian approach to predict the parameters of the distributions of wind speeds under the condition that there is limited measured wind speed data at the study site. Thus, the uncertainties in the air density, performance curve, and wind speeds at the reference site are both considered. For the stochastic approaches, there are different researches, *e.g.*, the Self-Exciting Threshold Autoregressive (SETAR) model by Gallego et al. [33] that is based on the Regime-Switching Autoregression (RS-AR) nonlinear time-series model, the Conditional Parametric Autoregression eXtraneous (CPARX) model by Nielsen [34], and the neural network by Sideratos and Hatzigiorgiou [35], the Autoregression-Generalized Autoregressive with Conditional Heteroscedasticity (AR-GARCH) model [36]. In the AI approaches, the AI is used again to predict the parameters for defining the distribution, *e.g.*, the approach that uses a feedforward neural network to predict wind energy output by Khosravi et al. [37].

As to the GLUE approaches within the category of the parametric approaches (as drawn in Figure 2), the uncertainty analysis for wind energy forecasting is conducted by incorporating the GLUE (generalized likelihood uncertainty estimation) method. Basically, in the GLUE method, a user-defined likelihood function is used to quantify the difference between the simulated and measured data [38], such that the simulated results with better accuracy can be emphasized. Thus, it is conceptually a mixture of the MC, AI, and stochastic approaches. The GLUE method has been used in many fields because of its simplicity for implementation and its demonstrated capability for uncertainty analysis,

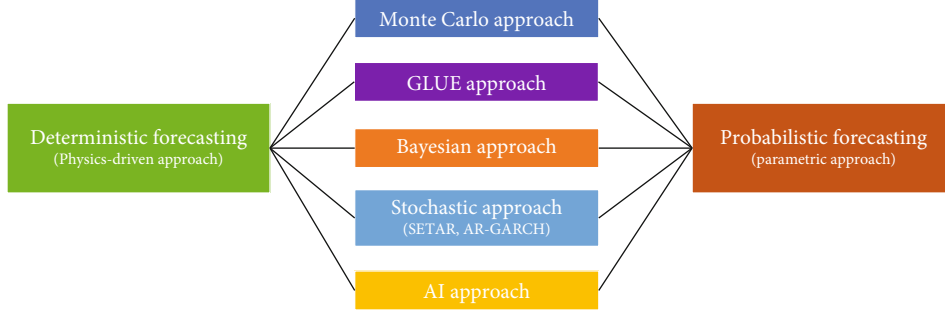


FIGURE 2: The illustration of the conversion from deterministic forecasting approaches (physics-driven approaches) to probabilistic forecasting approaches (parametric approaches).

e.g., in the hydrological models [39–41], flood inundation models [42–45], and rainfall-runoff models [46, 47], to access the uncertainties of studied problems. Nevertheless, currently, there is no research using the GLUE method to conduct the uncertainty analysis of wind energy generation.

To fill this gap, this study proposes a novel uncertainty analysis approach that couples the GLUE method with a deterministic forecasting approach to assessing the energy production of operational wind turbines at Penghu. Collected 10-year wind speed and energy output data of these wind turbines are utilized for this analysis. For demonstration, the data is divided into two 5-year data sets for the framework of execution and validation. The framework comprises 15 scenario testing cases with various time periods as twelve months, one strong-wind regime, one weak-wind regime, and one year to investigate the applicability of the GLUE method on long-term wind energy forecasting. For each testing case, the first 5-year data is utilized to analyze the uncertainties of the Weibull wind speed distribution parameters, the wind energy production, and the capacity factor by the GLUE method with two confidence intervals of 50% and 90%. Next, the framework is evaluated with the measured capacity factors based on the last 5-year data. To discover the advantages of the GLUE method, the MC method is selected for comparison because of its simplicity and applicability to various approaches. The results of the GLUE-based uncertainty analysis approach are compared with the results of the MC-based uncertainty analysis approach, and attention is devoted to the accuracy of the confidence intervals of wind energy output.

2. Deterministic Approach

2.1. Weibull Wind Speed Distribution (WWS D). In general, wind energy density per unit area can be estimated using a probability density distribution fitting to a set of wind speed data. Considering that the natural distribution of measured wind speeds often matches a Weibull shape [3], the Weibull density function comprising two parameters is used to represent wind energy density:

$$f(V) = \frac{k}{c} \left(\frac{V}{c} \right)^{k-1} e^{-(V/c)^k}, \quad (1)$$

where $f(V)$ is the wind energy density function, V is the wind speed (m/s), c is the scale parameter highly related to the mean of the wind speed distribution, and k is the shape parameter that is usually in a range between 1.5 and 3. The corresponding cumulative distribution function $F(V)$ can be obtained by integrating Equation (1):

$$F(V) = 1 - e^{-(V/c)^k}. \quad (2)$$

There are various ways to find the scale c and shape k parameters, i.e., the numerical approaches [48] and the artificial intelligence approaches [11, 49] with higher accuracy but heavier computational demands than the numerical approaches. For simplicity and acceptable accuracy in predicting the parameters (Chang et al. [7]), the maximum likelihood method as in the category of the numerical approach is used to compute the two parameters through iterations using the following equations [4]:

$$k = \left(\frac{\sum_{i=1}^n V_i^k \ln(V_i)}{\sum_{i=1}^n V_i^k} - \frac{\sum_{i=1}^n \ln(V_i)}{n} \right)^{-1}, \quad (3)$$

$$c = \left(\frac{1}{n} \sum_{i=1}^n V_i^k \right)^{1/k},$$

in which subscript i refers to the i^{th} time period and n is the number of nonzero measured wind speed data. The average wind speed \bar{V} at a local site is given by

$$\bar{V} = c\Gamma \left(1 + \frac{1}{k} \right), \quad (4)$$

where Γ denotes the Gamma function as $\Gamma(z) = (z-1)!$.

2.2. Wind Energy Production. Wind energy production is the process that converts the energy of wind into mechanical energy and stores the mechanical energy as power energy. Nevertheless, since there are several types of losses in the system, the whole mechanical energy cannot be completely converted into power energy. Currently, for estimating the energy output from a wind turbine at a specific wind speed, there are two commonly used approaches. In the first

approach, the energy output is computed by utilizing the standard performance curve from the manufacturers which describes the energy output at various wind speeds under a standard environment. The other approach estimates the energy output by the regression methods or artificial neural networks from the measured data set of wind speeds and energy output. Nevertheless, although the second approach can lead to higher accuracy than the first approach, it requires massive data for the computations. As a result, the present study adopts the first approach hereinafter to calculate the energy output of a wind turbine at a specific wind speed. The corresponding formula for determining the energy output by a standard performance curve is given as

$$P(V) = \begin{cases} 0, & V < V_1, \\ (a_0 + a_1 V + a_2 V^2 + a_3 V^3 + a_4 V^4)P_R, & V_1 \leq V < V_R, \\ P_R, & V_R \leq V < V_O, \\ 0, & V \geq V_O, \end{cases} \quad (5)$$

where V_1 , V_R , and V_O refer to the cut-in wind speed, rated wind speed (m/s), and cut-out wind speed (m/s), respectively. P_R is the rated power which is the maximum energy output of the wind turbine. a_0 , a_1 , a_2 , a_3 , and a_4 are coefficients that are provided by the corresponding manufacturer of the used wind turbine. From Equation (5), when the wind speed is less than the cut-in wind speed, the fans of the wind turbine are not rotated such that the subsequent energy output is zero. When the wind speed is greater than the cut-in wind speed, the fans of the wind turbine are rotated and the energy output is subsequently produced. Constant energy output (*i.e.*, the maximum energy output) is produced by the wind turbine under the condition that the wind speed is between the rated and cut-off wind speeds. When the wind speed is greater than the cut-off wind speed, the wind turbine is turned down to avoid potential permanent damage under such a violent wind; hence, there is no energy output. The standard performance curve is displayed in Figure 3 for illustration.

Combining the WWSD aforementioned in Section 2.1 and the standard performance curve in this subsection, the energy output (E_w) in a time period Δt can be expressed as

$$E_w = \Delta t \int_{V_1}^{V_O} P(V) f(V) dV, \quad (6)$$

which leads to the form of

$$E_w = \Delta t P_R \int_{V_1}^{V_R} (a_4 V^4 + a_3 V^3 + a_2 V^2 + a_1 V + a_0) \frac{k}{c} \left(\frac{V}{c}\right)^{k-1} e^{-(V/c)^k} dV + \Delta t P_R \int_{V_R}^{V_O} \frac{k}{c} \left(\frac{V}{c}\right)^{k-1} e^{-(V/c)^k} dV. \quad (7)$$

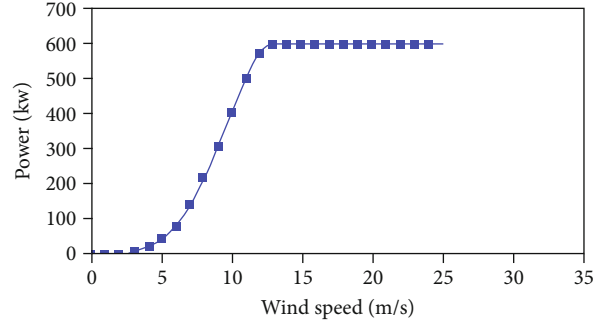


FIGURE 3: The standard performance curve. The standard performance curve of the Enercon E44-600KW wind turbine is used for giving an example.

Equation (7) is solved by applying numerical integration. In practice, the energy output E_w is often divided by the maximum energy output E_R to derive a dimensionless factor as the capacity factor C_F to give a more objective inspection of the produced energy output [3, 50]. Hence, the produced energy output is represented by the capacity factor hereinafter. The capacity factor C_F is defined as (Chang et al. [7])

$$C_F = \frac{E_w}{E_R}. \quad (8)$$

The formula for computing the capacity factor C_F can be deduced by combining Equations (7) and (8), leading to

$$C_F = \int_{V_1}^{V_R} (a_4 V^4 + a_3 V^3 + a_2 V^2 + a_1 V + a_0) \frac{k}{c} \left(\frac{V}{c}\right)^{k-1} e^{-(V/c)^k} dV + \int_{V_R}^{V_O} \frac{k}{c} \left(\frac{V}{c}\right)^{k-1} e^{-(V/c)^k} dV. \quad (9)$$

Equation (9) cannot be directly integrated. Instead, the present study adopts the recursive adaptive Simpson quadrature to numerically solve Equation (9) to find the capacity factor C_F .

3. Uncertainty Analysis Approaches

3.1. Generalized Likelihood Uncertainty Estimation (GLUE) Method. The GLUE method is currently one of the main methods used for uncertainty analysis in hydrology and water quality simulations [38]. It utilizes the likelihood function and considers the parameter space and probability distribution patterns to appropriately describe the involved physical mechanisms. Under general circumstances, as long as a model has several parameter combinations and measured simulation results, the analysis process can be initiated. The first step in performing the uncertainty analysis by the GLUE method is to decide a representative likelihood function that measures the difference between the simulated and measured results. Then, the decided likelihood function is used to perform a sensitivity analysis of all the involved

parameters. A likelihood value scatterplot of each involved parameter is conducted to observe where the optimal performance occurs. Subsequently, the parameter range for the parameter is determined. Then, a sufficiently large number of parameter combinations are created based on these derived parameter ranges. The simulated values and the corresponding likelihood values of these parameter combinations are computed and recorded. For a parameter combination, the likelihood value is updated when a new likelihood value is computed due to the use of new data:

$$L_i = w_0 L_0 + w_1 L_1, \quad (10)$$

where L_i is the updated likelihood value, L_0 refers to the likelihood value based on the original data, L_1 is the likelihood value based on the new data, and w_0 and w_1 are the weights for the original and new data, respectively. After the likelihood value of each parameter combination is computed and/or updated, the simulated results are then sorted according to the simulated value of each parameter combination. After that, the likelihood values are normalized to obtain the desired distribution. The confidence intervals are subsequently derived based on the distribution.

3.2. Monte Carlo (MC) Estimation Method. Monte Carlo simulation is a method for solving problems via massive random samplings to produce a huge number of simulations that can describe the desired population [51]. Nowadays, through the use of computers, a lot of samplings and corresponding simulations can proceed to obtain an estimated answer in a relatively short time. The MC method is currently being applied in many fields such as physics, chemistry, and even social sciences. The basic principle of the MC method is to define all possible events via the considered probability density functions and to cumulate the probability density functions into cumulative probability functions from 0 to 1. Through massive simulated data, a link can be established between random sampling and actual problem simulation. Then, the most likely result of an actual problem is conducted. According to the central limit theorem, the sample average after massive simulation is the unbiased estimation of the population's average. Also, the confidence interval can be obtained by statistically analyzing the outcomes of these simulations.

4. Study Site and Data Background

4.1. Analysis of Wind Speed and Power Data of Wind Turbines at the Study Site. This study uses measured data of wind speeds and power output at four Enercon E44-600KW wind turbines in the Jhongtun wind power station at Penghu which is an offshore island in the middle of the Taiwan Strait, as Figure 4(A) depicts. The Jhongtun wind power station has been operating since 2001. It is the second median-scale wind power plant in Taiwan and the first wind power plant located on the offshore island of Taiwan. The station is set in the Baisha village of Penghu, as Figure 4(B) displays. The four Enercon E44-600KW wind turbines are erected by the Taiwan Power Company on the north side

of the village, as depicted in Figure 4(C). The four wind turbines are marked as 1, 2, 3, and 4 from east to west in Figure 4(D). An Enercon E44-600KW wind turbine has a capacity of 600 kW with 3 m/s, 13 m/s, and 25 m/s for the cut-in, rated, and cut-off wind speeds, respectively. The parameters for the standard performance curve in Equation (5) are given as $a_0 = -0.2511$, $a_1 = 0.1794$, $a_2 = -0.04818$, $a_3 = 0.00621$, and $a_4 = -0.00023$. Time series of wind speeds and power output of the four wind turbines have been recorded in a 10-minute time resolution from 2002 to 2011. Unfortunately, after 2012, the measured data is no longer available to the public. Nevertheless, this situation will not influence the quality of the present paper. On the other hand, despite the measured data of the four wind turbines can all be adopted for the rest of uncertainty analysis, the records of the last three wind turbines are not used since the wind speeds around these three wind turbines are influenced by the first wind turbine (wind turbine #1) in the wind velocity field of northeast monsoon during the strong-wind regime (from October to March). Furthermore, the 10 min measured data of wind turbine #1 is shortened to 1-hour data by averaging the six 10 min data within an hour to increase the computational efficiency. In terms of the pattern of the wind velocity field, it can be classified as the strong-wind and weak-wind (from April to September) regimes. In the strong-wind regime, the wind speeds can be up to 10 m/s to 16 m/s, whereas the wind speeds are between 5 m/s and 10 m/s in the weak-wind regime. Therefore, to discover the capability of the developed uncertainty analysis in various timespans, the present study has 15 scenario testing cases, *i.e.*, twelve months, the strong-wind regime, the weak-wind regime, and one year. The obvious difference in the weak-wind and strong-wind regimes also leads to the difference in capacity factors [5], which can be seen in Table 1. Table 1 lists the monthly capacity factors determined by the 1-hour time series of each scenario during the 10 years. Table 1 also displays the estimated monthly capacity factors by the deterministic approach aforementioned in Section 2 where the measured wind speed data for each year is used to find the fitted Weibull distribution in each scenario. From Table 1, the aforementioned two prominent wind regimes can be inspected within a year in Taiwan. In the strong-wind regime, the monthly capacity factors are in the range of 0.509 to 0.793. On the other hand, the monthly capacity factors in the weak-wind regime are only between 0.188 and 0.373. Besides, it is seen that a larger discrepancy between the measured and estimated capacity factors is found in the weak-wind regime (up to 28.2%) than in the strong-wind regime (up to 8.2%). Such a phenomenon can also be seen in monthly scenarios. The average error for the scenario with weak wind (months from April to September) is in a range between 8.8% and 25.13%, and the average error for the scenario with strong wind (months from October to March) is between 3.3% and 18.7%. Thus, the above phenomenon indicates the necessity to use uncertainty analysis approaches to predict the capacity factor of wind turbine #1.

Finally, as aforementioned, there is a fitted Weibull distribution for each year in each scenario. Consequently, there are 150 fitted Weibull distributions in the present

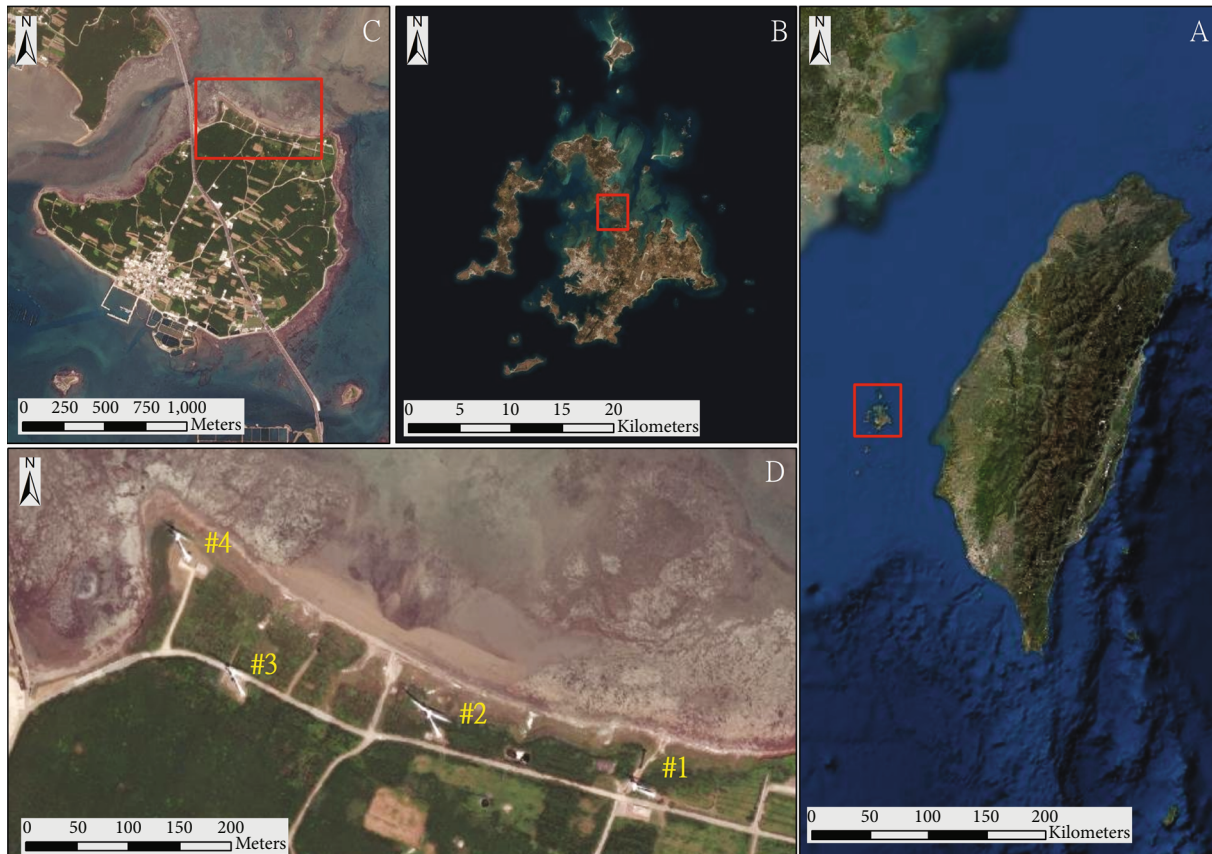


FIGURE 4: Locations of the four Enercon E44-600KW wind turbines installed in the Jhongtun wind power station. (A) The location of Penghu. (B) The location of the Baisha village where the Jhongtun wind power station is located on Penghu. (C) The location of the Jhongtun wind power station in Baisha village. (D) The locations of the four wind turbines of the Jhongtun wind power station.

study. Overall, these fitted Weibull distributions can all reasonably represent the distributions of the measured wind speeds provided that the coefficients of determination (R^2) are all acceptably close to 1. Owing to the space limitations, the fitted results for all 15 scenario testing cases in 2004 with an averaged R^2 of 0.81 are displayed in Figure 5 for demonstration. From this figure, regarding monthly scenarios, there might exist two peaks in a measured wind speed distribution where the wind speed turns from strong to weak or weak to strong (*i.e.*, February and October). This can also be seen in the one-year scenario where a peak for stronger winds and another peak for weaker winds are observed.

4.2. Uncertainty Analysis of the Wind Energy Production. In the present study, the prediction of the energy output of wind turbines through the adopted deterministic approach involves the determination of wind speeds by the WWSD and the wind-to-energy conversion through the performance curve of the wind turbines. As a result, the uncertainties of the wind energy output, which is represented by the capacity factor in the present study, are related to the WWSD and performance curve. Specifically, for the WWSD, the uncertainties come from the shape parameter k and scale parameter c , as will be discussed in Subsection 4.2.1. Nevertheless, the uncertainties in selecting the Weibull distribution instead of other distributions to describe wind speeds

are not considered in the present study since the Weibull distribution is proven to have the best fitness than the other distributions. The uncertainties of the WWSD and the performance curve are next discussed in Subsections 4.2.1 and 4.2.2, respectively. The distinctive procedures for implementing the MC and GLUE methods are introduced in Subsection 4.2.3 and 4.2.4, respectively.

4.2.1. Uncertainties of the WWSD. As the amount of wind speed data in the distribution selection process is often very large, a perfect description for the measured wind speed data by a probability density distribution is unable to be obtained. Chang et al. [3] collect wind speed data from 25 weather stations between 1996 and 1999 and find that the Weibull distribution coincides with the measured wind speed data with a high degree of precision. Furthermore, concerning the wind speed distribution in Taiwan, the Weibull distribution is again to be the most representative. Hence, this study selects the Weibull distribution to represent wind speed data, and the uncertainties in using the Weibull distribution instead of other distributions are not considered as aforementioned. Nevertheless, the uncertainties of the WWSD exist due to many factors. First, the anemometer is positioned behind the wind turbine's blades such that the wind turbine's slipstream or other wind turbines nearby may cause a draft disturbance. Also, human activities, machine

TABLE 1: The monthly estimated capacity factors based on Chang et al. [3] and measured capacity factors for wind turbine #1 between 2002 and 2011. The error is calculated as $|\text{measured}-\text{estimated}|/\text{measured}$.

Scenario	Variable	Year									
		2002	2003	2004	2005	2006	2007	2008	2009	2010	2011
January	Estimated	0.582	0.766	0.839	0.749	0.785	0.927	0.763	0.790	0.606	0.965
	Measured	0.621	0.752	0.822	0.743	0.809	0.941	0.802	0.773	0.661	0.983
	Error (%)	6.3%	1.9%	2.1%	0.8%	3.0%	1.5%	4.9%	2.2%	8.3%	1.8%
February	Estimated	0.595	0.526	0.567	0.627	0.680	0.492	0.915	0.462	0.464	0.630
	Measured	0.596	0.533	0.567	0.509	0.730	0.512	0.871	0.424	0.479	0.663
	Error (%)	0.2%	1.3%	0.0%	23.2%	6.8%	3.9%	5.1%	9.0%	3.1%	5.0%
March	Estimated	0.397	0.526	0.610	0.501	0.510	0.468	0.467	0.498	0.419	0.696
	Measured	0.396	0.542	0.661	0.202	0.527	0.454	0.453	0.530	0.449	0.743
	Error (%)	0.3%	3.0%	7.7%	148.0%	3.2%	3.1%	3.1%	6.0%	6.7%	6.3%
April	Estimated	0.368	0.362	0.360	0.283	0.347	0.420	0.363	0.472	0.438	0.313
	Measured	0.383	0.310	0.356	0.220	0.323	0.500	0.378	0.490	0.426	0.301
	Error (%)	3.9%	16.8%	1.1%	28.6%	7.4%	16.0%	4.0%	3.7%	2.8%	4.0%
May	Estimated	0.193	0.359	0.231	0.268	0.373	0.099	0.372	0.262	0.211	0.267
	Measured	0.184	0.345	0.217	0.206	0.315	0.099	0.323	0.298	0.229	0.222
	Error (%)	4.9%	4.1%	6.5%	30.1%	18.4%	0.0%	15.2%	12.1%	7.9%	20.3%
June	Estimated	0.154	0.357	0.350	0.238	0.148	0.115	0.138	0.217	0.356	0.160
	Measured	0.145	0.319	0.145	0.221	0.139	0.129	0.134	0.186	0.266	0.178
	Error (%)	6.2%	11.9%	141.4%	7.7%	6.5%	10.9%	3.0%	16.7%	33.8%	10.1%
July	Estimated	0.209	0.129	0.234	0.280	0.347	0.085	0.282	0.112	0.104	0.097
	Measured	0.196	0.117	0.204	0.176	0.258	0.091	0.228	0.114	0.115	0.119
	Error (%)	6.6%	10.3%	14.7%	59.1%	34.5%	6.6%	23.7%	1.8%	9.6%	18.5%
August	Estimated	0.154	0.132	0.210	0.189	0.122	0.274	0.064	0.236	0.051	0.176
	Measured	0.135	0.122	0.113	0.151	0.067	0.259	0.066	0.215	0.060	0.172
	Error (%)	14.1%	8.2%	85.8%	25.2%	82.1%	5.8%	3.0%	9.8%	15.0%	2.3%
September	Estimated	0.433	0.347	0.313	0.358	0.534	0.344	0.278	0.310	0.305	0.348
	Measured	0.384	0.347	0.337	0.277	0.390	0.354	0.309	0.331	0.298	0.369
	Error (%)	12.8%	0.0%	7.1%	29.2%	36.9%	2.8%	10.0%	6.3%	2.3%	5.7%
October	Estimated	0.556	0.670	0.927	0.792	0.737	0.765	0.571	0.759	0.697	0.791
	Measured	0.435	0.696	0.945	0.763	0.578	0.846	0.605	0.782	0.737	0.782
	Error (%)	27.8%	3.7%	1.9%	3.8%	27.5%	9.6%	5.6%	2.9%	5.4%	1.2%
November	Estimated	0.740	0.766	0.688	0.530	0.569	0.895	0.641	0.631	0.818	0.658
	Measured	0.709	0.779	0.725	0.597	0.545	0.913	0.380	0.703	0.820	0.706
	Error (%)	4.4%	1.7%	5.1%	11.2%	4.4%	2.0%	68.7%	10.2%	0.2%	6.8%
December	Estimated	0.750	0.820	0.886	0.876	0.887	0.710	0.735	0.727	0.623	0.919
	Measured	0.707	0.806	0.890	0.898	0.910	0.701	0.680	0.675	0.330	0.902
	Error (%)	6.1%	1.7%	0.4%	2.4%	2.5%	1.3%	8.1%	7.7%	88.8%	1.9%
Strong-wind	Estimated	0.596	0.672	0.747	0.672	0.687	0.693	0.667	0.636	0.590	0.777
	Measured	0.576	0.686	0.771	0.621	0.683	0.730	0.631	0.651	0.580	0.799
	Error (%)	3.5%	2.0%	3.1%	8.2%	0.6%	5.1%	5.7%	2.3%	1.7%	2.8%
Weak-wind	Estimated	0.261	0.296	0.289	0.279	0.318	0.250	0.278	0.282	0.262	0.242
	Measured	0.237	0.259	0.228	0.208	0.248	0.237	0.239	0.271	0.231	0.226
	Error (%)	10.1%	14.3%	26.8%	34.1%	28.2%	5.5%	16.3%	4.1%	13.4%	7.1%

TABLE 1: Continued.

Scenario	Variable	Year									
		2002	2003	2004	2005	2006	2007	2008	2009	2010	2011
One-year	Estimated	0.436	0.484	0.501	0.480	0.491	0.463	0.453	0.453	0.431	0.487
	Measured	0.406	0.472	0.499	0.414	0.465	0.483	0.435	0.461	0.405	0.512
	Error (%)	7.4%	2.5%	0.4%	15.9%	5.6%	4.1%	4.1%	1.7%	6.4%	4.9%

malfunction, or other issues may cause discrepancies between the measured and actual wind speeds. In the present study, the uncertainties of the WWSD are assumed to be mainly attributed to the uncertainties of the WWSD parameters which are obtained via measurement of the local long-term wind speeds, *i.e.*, the shape parameter k and scale parameter c . In such a way, the aforementioned discrepancy between the measured and actual wind speeds is reasonably included in the analysis.

4.2.2. Uncertainties of the Performance Curve. For a given wind speed, the energy output is obtained by substituting the wind speed into the performance curve provided by the wind turbine manufacturer or from the regression analysis of the measured data. However, these two methodologies are known to underestimate the monthly capacity factor in the strong-wind regime and overestimate the monthly capacity factor in the weak-wind regime [4]. Equivalently speaking, there is not yet a perfectly accurate method to determine the energy output. Consequently, the process of determining the capacity factor has some degree of uncertainty. Also, this process is subject to the limits imposed by the amplitude of the data, the size of the error in the model itself, and the errors due to human factors and machine malfunction. These involved uncertainties are all considered by accessing the uncertainties of the performance curve.

4.2.3. Procedures for the Uncertainty Analysis by the MC Method. In the adopted MC method, to consider the uncertainties within the WWSD (as the shape parameter k and scale parameter c) and the performance curve, for each scenario, a massive number of simulations are conducted via random sampling from 0 to 1 based on the cumulative density distributions of these parameters. The sequential procedures for creating a simulation for a specific scenario are introduced next.

In the first step, the uncertainties of the shape parameter k and scale parameter c in the WWSD are considered. Specifically, the uncertainties of the scale parameter c are herein considered by analyzing the uncertainties of the average wind speed \bar{V} . The shape parameter k and average wind speed are both assumed to be in normal distribution, and the statistics (*i.e.*, averages and standard deviations) of the two parameters in the scenario are computed by the 10-year measured data according to the period of the scenario. Based on the computed two normal distributions, a shape parameter k and an average wind speed are randomly sampled. Then, the sampled shape parameter k and average wind speed are utilized to compute the scale parameter c

through Equation (4). A WWSD $f(V)$ and its cumulative density function $F(V)$ are thus decided based on the shape parameter k and scale parameter c .

In the second step, a wind speed V is randomly sampled based on $F(V)$. Then, the capacity factor of wind turbine #1 is computed by using the performance curve based on the sampled wind speed V by Equation (9). To consider the uncertainties of the performance curve, the present study assumes that the energy output under a given wind speed V is a normal distribution. To find this normal distribution, the measured wind speeds and energy output in the Jhongtun wind plant are drawn in Figure 6. As shown in this figure, under a given wind speed, the distribution of the energy output is almost symmetrical despite some data being far away from the performance curve due to manual or mechanical problems. Hence, the present study assumes that the energy output is in the normal distribution under a given wind speed. The uncertainties of the performance curve are considered by assuming that the energy output on the performance curve is the average value of the normal distribution. Also, the standard deviation of the distribution is given as the variance of the measured energy output. For the variance of the measured energy output, it is assumed to be a negative-slope straight line between the cut-in and rated wind speeds and a horizontal line between the rated and cut-off wind speeds [28]. By analyzing the measured data in the Jhongtun wind plant, the coefficient of variation is computed and a regression curve is found (Figure 7(a)). Correspondingly, the standard deviation of the energy distribution ($\sigma_P(V)$) is given as

$$\sigma_P(V) = \begin{cases} \bar{P}(V) \times [0.1818 - 0.2823((V - V_R)/(V_R - V_I))], & V_I \leq V \leq V_R, \\ \bar{P}(V) \times 0.1818, & V_R \leq V \leq V_O, \end{cases} \quad (11)$$

where $\bar{P}(V)$ is the computed energy output under a given wind speed V from the standard performance curve. Thus, for a sampled wind speed V , the corresponding energy output is computed by the performance curve and then added by a deviation that is randomly sampled from a normal distribution with zero mean and a standard deviation of $\sigma_P(V)$. Taking the used Enercon E44-600KW wind turbine as an example, the generated energy output using the normal distribution together with Equation (11) is displayed in Figure 7(b). By repeating step 2 many times, the capacity factor can be computed. Finally, for the considered scenario, steps 1 and 2 are repeated 100,000 times to produce 100,000 capacity factors that can be used to derive the confidence

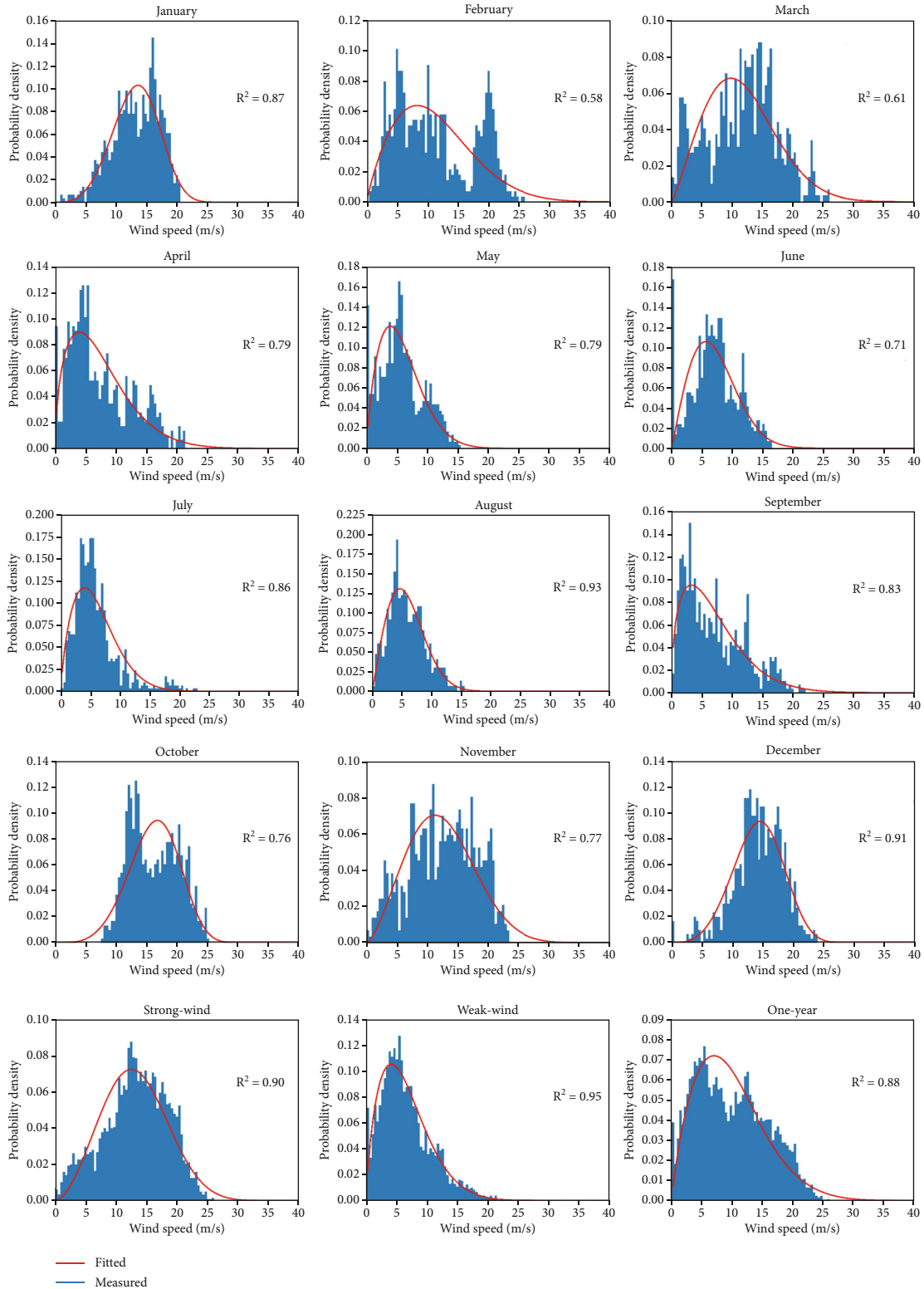


FIGURE 5: The 10 fitted Weibull wind speed distributions of the 15 scenario testing cases in 2004 of the Enercon E44-600KW wind turbine in Jhngtun.

interval of the capacity factor. The results for all 15 scenarios are displayed and analyzed in Section 5. The flowchart of the M-C method is displayed in Figure 8 for illustration.

4.2.4. Procedures for the Uncertainty Analysis by the GLUE Method. To implement the GLUE method for accessing the uncertainties of the energy output, the present study

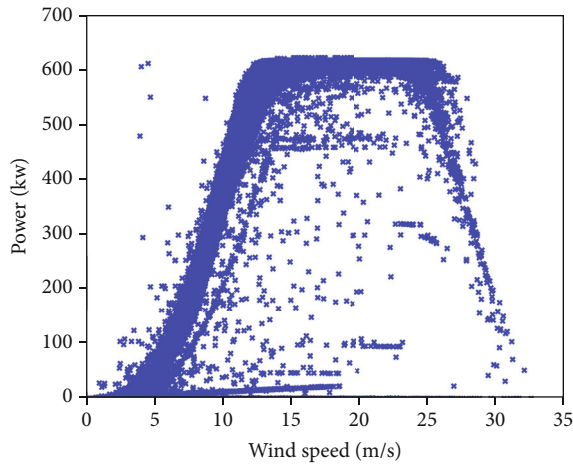


FIGURE 6: The measured performance curve of the installed Enercon E44-600KW wind turbine in Jhongtun.

modifies the formula presented by Nash and Sutcliffe [52] as the likelihood function since each simulated capacity factor is a single value [53]:

$$L = 1 - \left| \frac{X_s - X_o}{X_o} \right|, \quad (12)$$

where L is the likelihood value, X_s is the simulated value, and X_o is the measured value. As Equation (12) depicts, this likelihood function is 1 minus the corresponding error value. As a result, the likelihood value has a similar effect as the efficiency coefficient which represents the quality of the simulation result. After determining the likelihood function, the GLUE method then processes a parameter sensitivity analysis of the three considered parameters (the shape parameter k , scale parameter c , and performance curve) by using the likelihood values of all possible parameter combinations to discover the parameter range of each parameter that can lead to a simulated result with better accuracy. Although each scenario can have its determined parameter ranges, for the sake of simplicity, the parameter ranges are decided to have the best accuracy in all 15 scenarios. Usually, to discern the variation of the likelihood value in the simulation result, a larger parameter range will be used. Furthermore, to lower the complexity of using the GLUE method, the parameter range is defined by two ratios that describe the lower and upper bounds, respectively. In this way, concerning the shape parameter k , the parameter sensitivity analysis finds the optimal parameter range as $\alpha_1 k \sim \alpha_2 k$. Similarly, for the scale parameter c , the optimal parameter range is defined as $\beta_1 c \sim \beta_2 c$. The uncertainties of the performance curve are considered by multiplying a computed capacity factor with an adjusted coefficient γ . The parameter range of the performance curve is actually the parameter range of this coefficient as $\gamma_1 \sim \gamma_2$.

After finding the parameter ranges of the three uncertain parameters, for each scenario, the GLUE method separates the measured data into the training set (2002 to 2006) and the validation set (2007 to 2011) to demonstrate the predict-

ability of the GLUE-based approach. In the training set, for each year, the GLUE method randomly samples N_1 values of k parameter and N_2 values of c parameters from their corresponding parameter ranges with the assumption that k and c are both in uniform distribution. Subsequently, there are $N_1 \times N_2$ distinctive WSDs and corresponding capacity factors computed by Equation (9). Next, to include the uncertainties of the performance curve, N_3 values of the adjusted coefficients are randomly sampled with the same assumption that the adjusted coefficient is in uniform distribution. The previously computed $N_1 \times N_2$ capacity factors are multiplied by these N_3 adjusted coefficients, resulting in $N_4 = N_1 \times N_2 \times N_3$ parameter combinations and their corresponding capacity factors. After that, the likelihood values of these parameter combinations are computed. In the next step, for each parameter combination, an average likelihood value over the 5 years in the training stage is calculated by the following equation that is modified from Equation (10):

$$L_{avg,j} = w_{2002}L_{2002,j} + w_{2003}L_{2003,j} + w_{2004}L_{2004,j} + w_{2005}L_{2005,j} + w_{2006}L_{2006,j}, \quad j \in \{1 \cdots N_4\}, \quad (13)$$

where subscript j refers to the j^{th} parameter combination. The weights in Equation (13) (w_{2002} , w_{2003} , w_{2004} , w_{2005} , and w_{2006}) are all given as 1/5 based on the assumption that each year is an independent event. The flowchart in Figure 9 for illustration. In the validation set, as displayed in Figure 10, the GLUE method also creates N_4 parameter combinations and computes the corresponding capacity factors by the same means as the training set. The average likelihood values from the training stage are directly used as the likelihood values for these parameter combinations in the validation stage. These likelihood values are then utilized as the weights of these parameter combinations. In such a way, the probability and cumulative density functions of the capacity factor are established and the confidence interval of the capacity factor for the last 5-year validation set can be derived. The results of all the scenarios are discussed in Section 5.

5. Results and Discussion

In the present study, the MC and GLUE methods are used to establish the confidence intervals of the capacity factor of wind turbine #1 at the Jhongtun wind power station for the 15 scenario testing cases. For demonstration, for each scenario, the 50% and 90% confidence intervals of the two uncertainty analysis approaches are compared with the measured capacity factors in 2007-2011 to examine the applicability of the two approaches. Theoretically, when the established distribution of capacity factor is reasonable, there should be about two or three measured capacity factors falling within the 50% confidence interval of the distribution and about four or five measured capacity factors falling within the 90% confidence interval. The larger the number

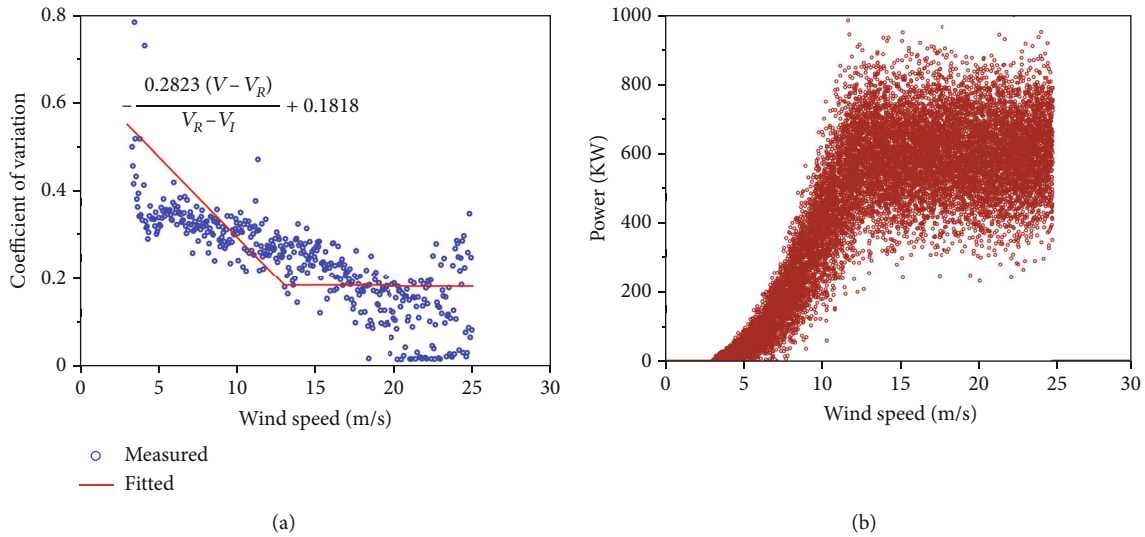


FIGURE 7: (a) The coefficient of variation for the Enercon E44-600KW wind turbine in Jhongtun. The blue circle is the computed coefficient of variation. The black lines are the regressed curve that consists of a negative slope and horizontal line segments. (b) The generated power curve from the normal distribution with a standard deviation of Equation (11).

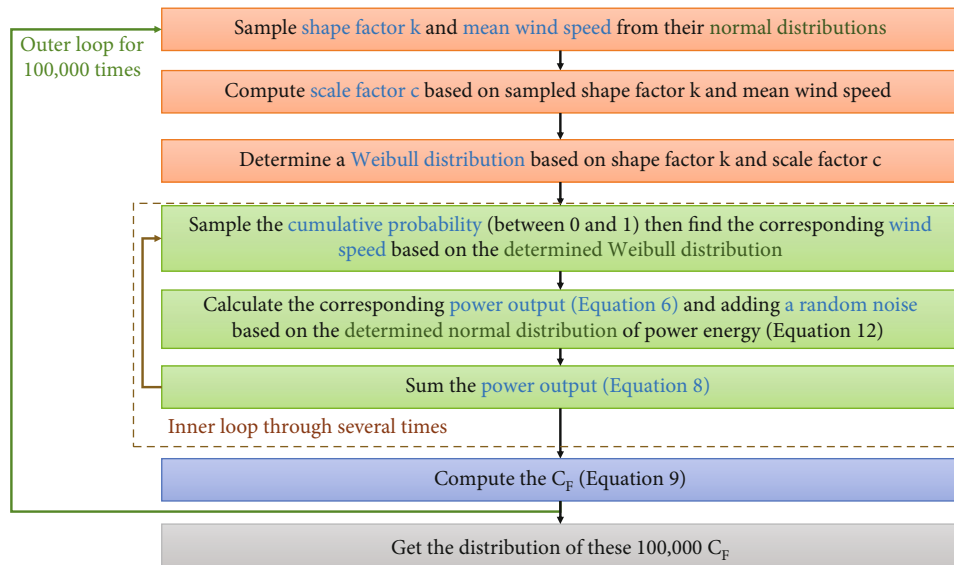


FIGURE 8: The flowchart of the M-C method for accessing the uncertainty of wind energy output in the present study.

of the measured capacity factors falling within the confidence interval is, the more the accuracy of the uncertainty analysis approach is. The results of the MC-based and GLUE-based uncertainty analysis approaches are displayed in subsections 5.1 and 5.2, respectively. The comparison between the two uncertainty analysis approaches is stated in subsection 5.3.

5.1. Results of the MC-Based Uncertainty Analysis Approach. The 50% and 90% confidence intervals of the capacity factor for all 15 scenarios of the MC-based approach are drawn in Figure 11. Overall, the MC-based approach can give accept-

ably accurate predictions in all 15 scenario testing cases. Specifically, in terms of the monthly scenarios, when concerning the 90% confidence interval, the MC-based approach can provide quite good predictions in January to May, July, and October. Particularly, the MC-based approach gives a satisfactory prediction in October. Nevertheless, in terms of the 50% confidence interval, the MC-based approach gives relatively poor predictions in almost all the months except April, August, October, and November. Specifically, in March and September, all the measured capacity factors are out of the 50% confidence interval. Comprehensively speaking, the MC-based approach provides relatively better

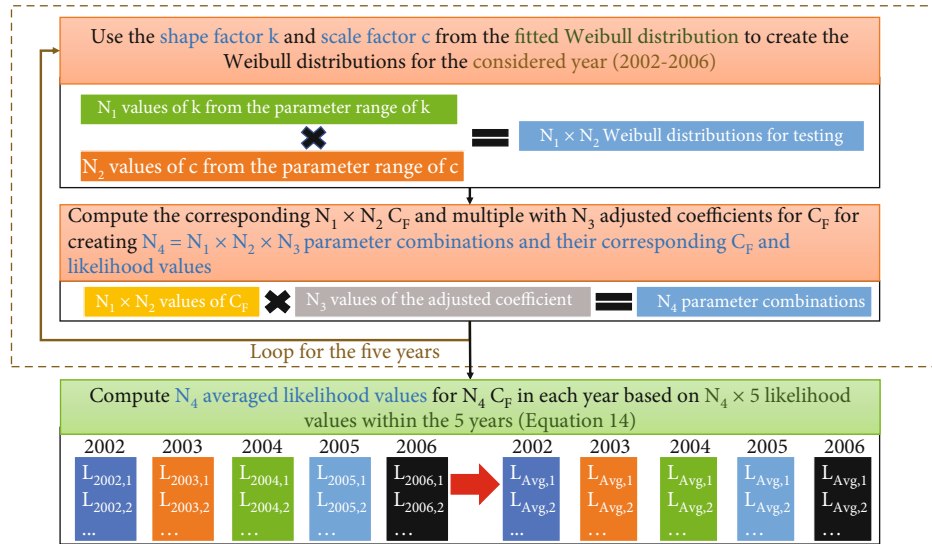


FIGURE 9: The flowchart in the training set of the GLUE method for accessing the uncertainty of wind energy output in the present study.

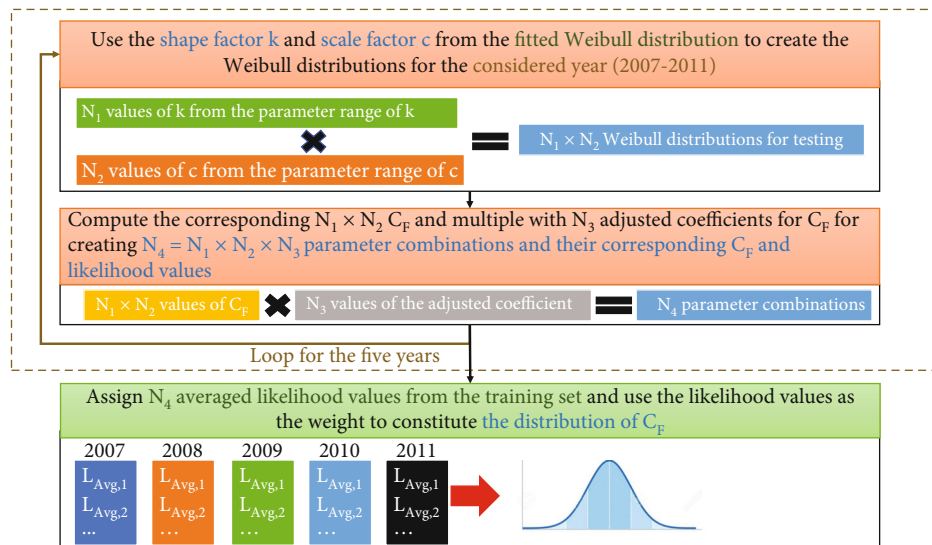


FIGURE 10: The flowchart in the validation set of the GLUE method for accessing the uncertainty of wind energy output in the present study.

results in April and October in which the weak/strong winds are changed into strong/weak winds. In other months, the accuracy of the MC-based approach on the confidence intervals, particularly for the 50% confidence interval, is relatively low. In terms of the strong-wind, weak-wind, and one-year scenarios, it is found that almost every measured capacity factor is out of the ranges of the 50% and 90% intervals, especially for the weak-wind and one-year scenarios. Also, the MC method tends to overestimate the capacity factors in all three scenarios, which is also seen in monthly scenarios with strong winds. Concerning the differences among the three scenarios, the 50% and 90% intervals in the weak-wind and one-year scenarios are both relatively narrower than the strong-wind scenario.

The above result indicates that the MC-based uncertainty analysis approach underestimates the uncertainty in

the three scenarios compared to the other monthly scenarios, especially in the weak-wind and one-year scenarios. Also, the MC-based approach tends to overestimate the capacity factors in all scenarios. The above phenomenon may be attributed to the use of the Weibull wind speed distribution and standard performance curve for wind-to-power conversion. In the present study, the two-parameter Weibull distribution is adopted such that the wind speed distributions in scenarios with more than one significant wind speed peak cannot be completely considered. Also, the Weibull wind speed distribution may significantly overestimate the capacity factors in the weak-wind periods and slightly underestimate the capacity factors in the strong-wind periods, as reported in [4]. Besides, there may still be unresolved uncertainty in the wind-to-power conversion by the standard performance curve. Nevertheless, the MC-

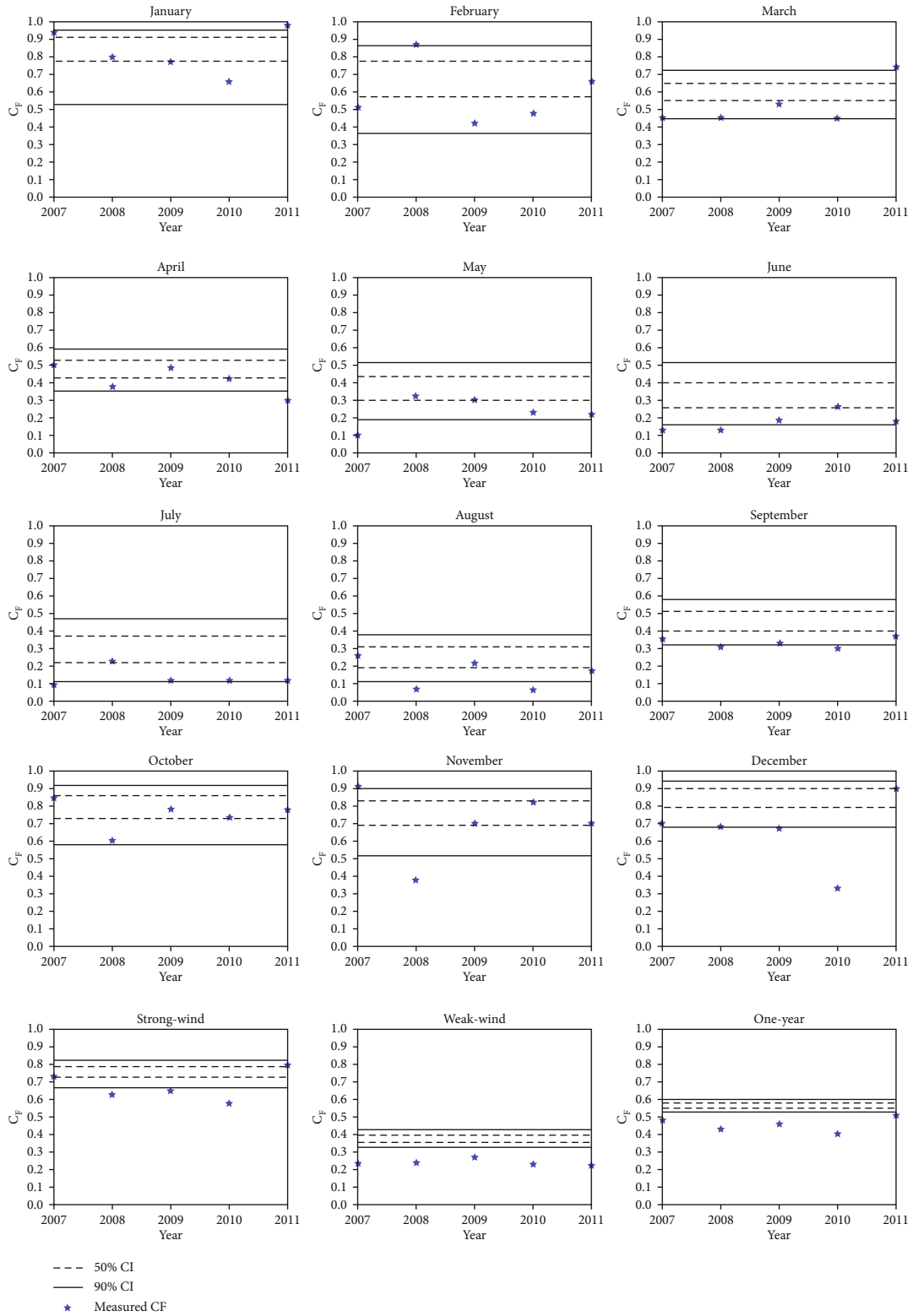


FIGURE 11: The 50% and 90% confidence intervals of the capacity factor (C_F) for the MC-based uncertainty analysis approach. The measured capacity factors during 2007-2011 are drawn for validation.

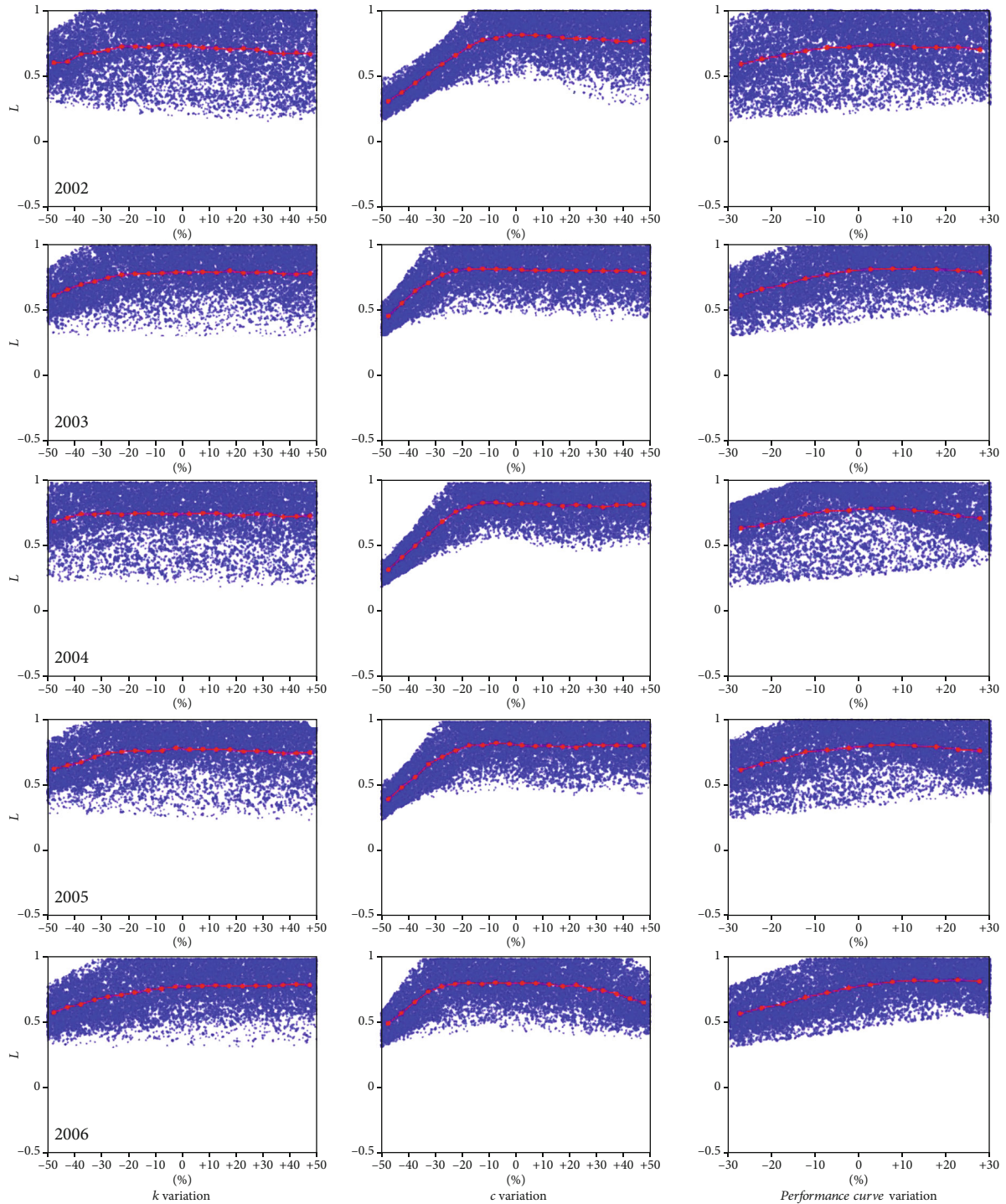


FIGURE 12: The parameter sensitivity analysis of k , c , and the performance curve in the monthly scenario for January. The trend of the likelihood values is representative of the scenarios with strong winds (the monthly scenarios from October to March and the strong-wind scenario).

based uncertainty analysis approach can still provide an acceptably accurate estimation of the wind power energy uncertainties.

5.2. Results of the GLUE-Based Uncertainty Analysis Approach

5.2.1. Parameter Sensitivity Analysis. For the parameter sensitivity analysis of the GLUE method, the values of the shape parameter k , scale parameter c , and adjusted coefficient of the performance curve range from -50% to +50% ($\alpha_1 = 0.5$ and $\alpha_2 = 1.5$), -50% to +50% ($\beta_1 = 0.5$ and $\beta_2 = 1.5$), and -30% to +30% ($\gamma_1 = 0.7$ and $\gamma_2 = 1.3$), respectively. Only

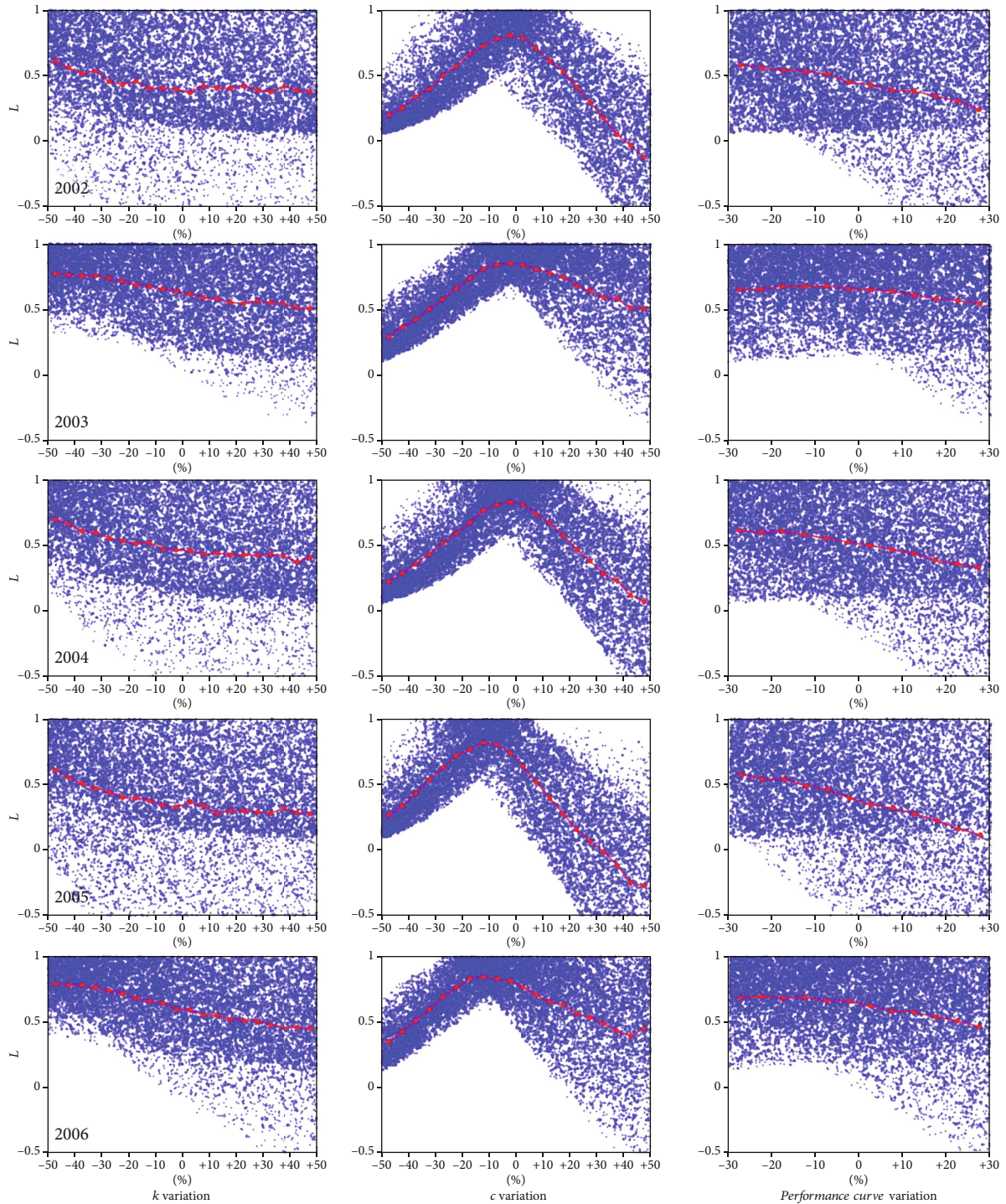


FIGURE 13: The parameter sensitivity analysis of k , c , and the performance curve in the monthly scenario for May. The trend of the likelihood values L is representative of the scenarios with weak winds (the monthly scenarios from April to September and the weak-wind scenario).

the data in the training set (2002 to 2006) is used for this analysis, and there are 10,000 simulations in each scenario. It is noted that the computed capacity factor is limited to be less than or equal to 1 to avoid unrealistic results. The closer the corresponding likelihood value (by Equation (12)) is to 1, the better the simulation result is. Based on the computed likelihood values in all of the 15 scenarios,

the optimal parameter ranges for the three parameters can be found. Owing to the space limitations, the results of the strong-wind and weak-wind scenarios are displayed in Figures 12 and 13, respectively, for showing the observed trends. The red dots in these figures are the averaged likelihood values used to depict the average trend of the likelihood value.

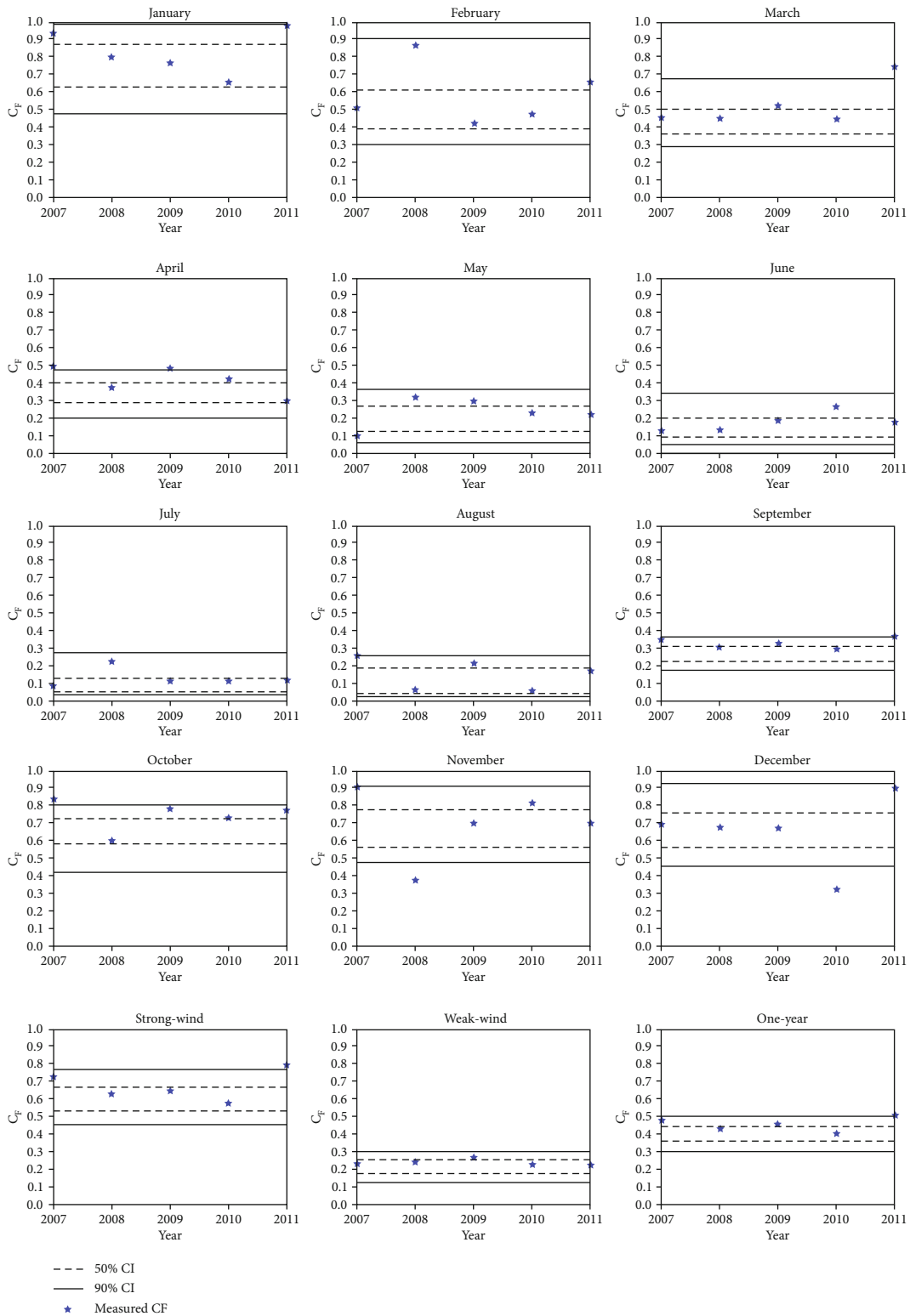


FIGURE 14: The 50% and 90% confidence intervals of the capacity factor (C_p) for the GLUE-based uncertainty analysis approach. The measured capacity factors during 2007-2011 are drawn in the figure as the “Measured CF” for validation.

Generally, concerning the distributions of likelihood values, for each parameter, the values of likelihood functions are concentrated to 1 in the strong-wind scenario, which is also seen in the monthly scenarios with strong wind (Janu-

ary to March and October to December). On the other hand, the weak-wind scenario and the weak-wind monthly scenarios (April to September) all have wider distributions of the likelihood values than in the strong-wind scenario and

TABLE 2: The number of measured capacity factors within the 50% and 90% confidence intervals of using the MC-based and GLUE-based approaches for the 15 scenario testing cases.

Scenario	MC-based						GLUE-based					
	CI = 50%			CI = 90%			CI = 50%			CI = 90%		
	$C_{F_{\text{libd}}}$	$C_{F_{\text{ubd}}}$	Count	$C_{F_{\text{libd}}}$	$C_{F_{\text{ubd}}}$	Count	$C_{F_{\text{libd}}}$	$C_{F_{\text{ubd}}}$	Count	$C_{F_{\text{libd}}}$	$C_{F_{\text{ubd}}}$	Count
January	0.777	0.911	1	0.533	0.954	4	0.639	0.876	3	0.484	0.993	5
February	0.575	0.777	1	0.361	0.862	4	0.392	0.615	3	0.302	0.910	5
March	0.551	0.651	0	0.448	0.720	4	0.366	0.507	3	0.292	0.681	4
April	0.433	0.528	2	0.350	0.591	4	0.291	0.407	2	0.203	0.474	3
May	0.305	0.437	1	0.193	0.519	4	0.128	0.272	2	0.055	0.364	5
June	0.255	0.407	1	0.158	0.510	3	0.092	0.203	4	0.052	0.345	5
July	0.216	0.369	1	0.112	0.469	4	0.056	0.130	4	0.034	0.277	5
August	0.193	0.311	2	0.107	0.382	3	0.044	0.192	3	0.022	0.258	4
September	0.398	0.509	0	0.320	0.584	3	0.226	0.313	2	0.173	0.371	5
October	0.733	0.863	4	0.587	0.915	5	0.588	0.728	1	0.426	0.808	4
November	0.690	0.835	3	0.517	0.901	3	0.565	0.782	2	0.484	0.918	4
December	0.795	0.902	0	0.676	0.941	3	0.568	0.761	3	0.455	0.938	4
Strong-wind	0.723	0.791	1	0.667	0.826	2	0.538	0.672	3	0.458	0.771	4
Weak-wind	0.356	0.396	0	0.326	0.423	0	0.178	0.259	4	0.133	0.304	5
One-year	0.550	0.580	0	0.526	0.600	0	0.359	0.445	2	0.301	0.500	4

monthly with strong wind. As for the one-year scenario, its pattern of likelihood values lies between the strong-wind and weak-wind scenarios. Based on these results, to simultaneously get high likelihood values in all the scenario testing cases, the parameter ranges for k , c , and the performance curve are determined to be -20% to +10%, -30% to +10%, and -10% to 10%, respectively. Equivalently speaking, $\alpha_1 = 0.8$ and $\alpha_2 = 1.1$ for the parameter range of k , $\beta_1 = 0.7$ and $\beta_2 = 1.1$ for the parameter range of c , and $\gamma_1 = 0.9$ and $\gamma_2 = 1.1$ for the parameter range of the adjusted coefficient. On the other hand, the shape parameter c is found to be the most sensitive, while the uncertainties of the performance curve are almost neglectable. In terms of the uncertainties in different scenarios, the uncertainties in the weak-wind regime are relatively larger than in the strong-wind regime.

5.2.2. Uncertainty Analysis. The GLUE method conducts the uncertainty analysis by using the determined parameter ranges of the three considered parameters, as discussed in subsection 5.2.1. The analyzed outcomes of the GLUE method are displayed in Figure 14.

From the viewpoint of the monthly scenarios, concerning the 90% confidence interval, the GLUE method leads to accurate results in almost all months except April. As for the 50% confidence, the GLUE method only fails in October where only one measured capacity factor is within the 50% confidence interval. Thus, when simultaneously concerning the performance on the 50% and 90% confidence intervals, the accuracy of the GLUE method is quite good except for April and October. For the strong-wind, weak-wind, and one-year scenarios, the GLUE method also successfully maintains its high accuracy on both the two confidence intervals in which sufficient numbers of the measured

capacity factors fall within the intervals. The reason why the results in April and October are less accurate is because the two months fall in either spring or autumn, a time when both strong/weak winds meet and bring greater fluctuations in wind speeds. Nevertheless, if the time scale is extended to 6 months for the strong-wind, weak-wind, or even one-year scenarios, the differences in the annual capacity factors are small since the homogeneity of the data is increasing.

5.3. Performance Comparison between the MC-Based and GLUE-Based Approaches. For comparing the two approaches, for each scenario, the numbers of the measured capacity factors, as listed in Table 1, that fall within the 50% and 90% confidence intervals are counted and listed in Table 2. The lower and upper bounds of the capacity factor (denoted as $C_{F_{\text{libd}}}$ and $C_{F_{\text{ubd}}}$, respectively) for the two approaches are also listed in Table 2 for illustration. Furthermore, a visual comparison is also conducted by inspecting Figures 11 and 14. Based on Table 2 and the two figures, both two approaches are found to provide acceptably accurate estimations of the wind energy output uncertainties. Nevertheless, the GLUE-based approach provides results that match the measured data better than the MC-based approach. When considering the monthly scenarios, the GLUE-based approach gives pretty accurate results in almost all months except for April and October in which the numbers of the measured capacity factors in the 50% or 90% confidence intervals are relatively smaller. Compared to the GLUE-based approach, the MC-based approach only gives the same accurate results in April and October. In other months, the 50% and 90% confidence intervals, particularly for the 50% confidence intervals, are found to be less consistent with the measured. Specifically, there is no measured capacity factor falling

within the 50% confidence intervals in March and September.

Regarding the strong-wind scenario, the GLUE-based approach has 3 and 4 data points within the 50% and 90% confidence intervals, respectively, which demonstrates the capability of the GLUE-based approach to grasp the degree of variations in the capacity factor. For the MC-based approach, there are only 1 and 2 measured capacity factors falling within the 50% and 90% confidence intervals, respectively. Hence, compared to the GLUE-based approach, the variations of capacity factors are relatively underestimated by the MC-based approach. Also, inspection of Figures 11 and 14 and Table 2 indicates that the confidence intervals by the MC-based approach are relatively narrower than the GLUE-based approach. This result means that the MC-based approach relatively underestimates the degree of uncertainty. For the weak-wind scenario, almost all measured capacity factors fell within the 50% and 90% confidence intervals of the GLUE-based approach. The simulation results of the MC-based approach are found to be distorted given that no measured capacity factor is within the 50% and 90% confidence intervals. For the one-year scenario, the GLUE-based approach has 2 and 4 measured capacity factors that fell within the 50% and 90% confidence intervals, respectively, which is good. The simulation results of the MC-based approach are found to be distorted again provided that no measured capacity factor is found to fall within the two confidence intervals.

In summary, whether using the quantitative method to calculate the number of measured capacity factors falling within the confidence intervals or conducting a direct comparison through graphs, despite the MC-based and GLUE-based approaches are both considered to be accurate enough, the simulation results of the GLUE-based approach are relatively superior to the MC-based approach. The former produces relatively better simulation results in each simulated scenario. Also, in some scenarios in which the MC-based approach estimates distorted results, the GLUE-based approach is still able to grasp the measured capacity factor. In light of this, the simulation results of the GLUE-based approach meet the actual uncertainties of the capacity factor better than the MC-based approach in the selected wind power station. This result is mainly attributed to the fact that the GLUE method has verification procedures whereas the MC method does not. In the GLUE method, the likelihood value that measures the difference between the simulated and measured data is used as the weight such that better-simulated results can be efficiently selected and emphasized. For the MC method, it may lead to results that are less consistent with the measured data, which is due to the use of the WWS and unresolved uncertainty in the wind-to-power conversion. The adopted WWS cannot completely represent the wind speed distributions in scenarios with more than one wind speed peak (e.g., one-year scenario). Also, the WWS may significantly overestimate the capacity factors in weak-wind periods and slightly underestimate the capacity factors in strong-wind periods, as found by [4]. Finally, there may be unresolved uncertainties in the wind-to-power conversion by the standard performance

curve. On the other hand, when the steps of simulations are lengthened, the MC method is not only time-consuming but also inefficient. In contrast, in the GLUE method, other events can directly use the previous results and effectively obtain an appropriate amount of data. Thus, the GLUE method is more effective to be implemented than the MC method.

6. Conclusions

This study combines the GLUE method with a deterministic forecasting approach to propose a novel uncertainty analysis approach for wind energy forecasting. The 10-year measured wind speed and energy output data of operational wind turbines in the Jhongtun wind farm at Penghu located in the middle of the Taiwan Strait is collected and divided into two 5-year data sets for the framework of execution and validation to demonstrate the GLUE method. To thoroughly discover the performance of the proposed uncertainty analysis approach in forecasting long-term wind energy output, there are 15 scenarios testing cases with various time periods (twelve months, the strong-wind regime, the weak-wind regime, and one year) in the framework. In the execution framework, the uncertainties in the wind speed distribution, performance curve, and capacity factors are accessed by the GLUE method. Next, the framework is validated by comparing the 50% and 90% confidence intervals of the wind energy output with the measured capacity factors in the last 5-year data. Besides, the proposed framework is compared with the results of the uncertainty analysis approach by the MC method. Based on the results, some conclusions are given as follows.

First, it is found that both the two uncertainty analysis approaches can give acceptably accurate predictions of 50% and 90% confidence intervals. Nevertheless, both 50% and 90% confidence intervals of the proposed uncertainty analysis approach are found to be more consistent with the measured capacity factors than the MC-based uncertainty analysis approach in all the considered scenarios. Specifically, the MC-based approach even has some undesired distortion in the weak-wind and one-year scenarios whereas the proposed approach still behaves well. On the other hand, concerning the performance of the proposed approach in various scenarios, the results reveal that the accuracy in April and October is relatively less than those in the other months because of relatively greater wind speed fluctuations in these two months. Overall, the proposed uncertainty analysis approach is demonstrated to provide relatively better simulation results than the MC-based approach, indicating that the GLUE method is relatively more efficient in conducting the uncertainty analysis of wind energy data and their distribution.

Data Availability

The result of the study is available from the corresponding author under request.

Conflicts of Interest

The authors declare that there is no conflict of interest regarding the publication of this paper.

Acknowledgments

The authors are grateful for the financial support of this work partially provided by the National Science and Technology Council, Taiwan, under Grant No. 112-2625-M-002-023.

References

- [1] A. Al-Quraan, H. Darwish, and A. M. A. Malkawi, "Renewable energy role in climate stabilization and water consumption minimization in Jordan," *PRO*, vol. 11, no. 8, article 2369, pp. 1–30, 2023.
- [2] GWEC, *Global Wind Statistics 2022*, Global Wind Energy Council, 2023.
- [3] T. J. Chang, Y. Y. Wu, H. Y. Hsu, C. R. Chu, and C. M. Liao, "Assessment of wind characteristics and wind turbine characteristics in Taiwan," *Renewable Energy*, vol. 28, no. 6, pp. 851–871, 2003.
- [4] T. J. Chang and Y. L. Tu, "Evaluation of monthly capacity factor of WECS using chronological and probabilistic wind speed data: a case study of Taiwan," *Renewable Energy*, vol. 32, no. 12, pp. 1999–2010, 2007.
- [5] Y. L. Tu, T. J. Chang, C. I. Hsieh, and J. Y. Shih, "Artificial neural networks in the estimation of monthly capacity factors of WECS in Taiwan," *Energy Conversion and Management*, vol. 51, no. 12, pp. 2938–2946, 2010.
- [6] Y. L. Tu, T. J. Chang, C. L. Chen, and Y. J. Chang, "Estimation of monthly wind power outputs of WECs with limited record period using artificial neural networks," *Energy Conversion and Management*, vol. 59, pp. 114–121, 2012.
- [7] T. J. Chang, C. L. Chen, Y. L. Tu, H. T. Yeh, and Y. T. Wu, "Evaluation of the climate change impact on wind resources in Taiwan Strait," *Energy Conversion and Management*, vol. 95, pp. 435–445, 2015.
- [8] Y. T. Wu, C. Y. Lin, and T. J. Chang, "Effects of inflow turbulence intensity and turbine arrangements on the power generation efficiency of large wind farms," *Wind Energy*, vol. 23, no. 7, pp. 1640–1655, 2020.
- [9] J. Yan, C. Möhrlein, T. Göçmen, M. Kelly, A. Wessel, and G. Giebel, "Uncovering wind power forecasting uncertainty sources and their propagation through the whole modelling chain," *Renewable and Sustainable Energy Reviews*, vol. 165, p. 12519, 2022.
- [10] Y. Zhang, J. Wang, and X. Wang, "Review on probabilistic forecasting of wind power generation," *Renewable and Sustainable Energy Reviews*, vol. 32, pp. 255–270, 2014.
- [11] A. Al-Quraan, B. Al-Mhairat, A. M. A. Malkawi, and A. Radaideh, "Optimal prediction of wind energy resources based on WOA-A case study in Jordan," *Sustainability*, vol. 15, no. 5, article 3927, pp. 1–23, 2023.
- [12] C. McGowin, *California wind energy forecasting system development and testing. Phase 1: initial testing*, Electric Power Research Institute (EPRI), Palo Alto, California, 2003.
- [13] M. Lie, L. Shiyang, J. Chuanwen, L. Hongling, and Z. Yan, "A review on the forecasting of wind speed and generated power," *Renewable and Sustainable Energy Reviews*, vol. 13, no. 4, pp. 915–920, 2009.
- [14] H. Liu, C. Chen, X. Lv, X. Wu, and M. Liu, "Deterministic wind energy forecasting: a review of intelligent predictors and auxiliary methods," *Energy Conversion and Management*, vol. 195, pp. 328–345, 2019.
- [15] C. D. Zuluaga, M. A. Alvarez, and E. Giraldo, "Short-term wind speed prediction based on robust Kalman filtering: an experimental comparison," *Applied Energy*, vol. 156, pp. 321–330, 2015.
- [16] Y. Wang, Z. Xie, Q. Hu, and S. Xiong, "Correlation aware multi-step ahead wind speed forecasting with heteroscedastic multi-kernel learning," *Energy Conversion and Management*, vol. 163, pp. 384–406, 2018.
- [17] H. Liu, X. W. Mi, and Y. F. Li, "An experimental investigation of three new hybrid wind speed forecasting models using multi-decomposing strategy and ELM algorithm," *Renewable Energy*, vol. 123, pp. 694–705, 2018.
- [18] P. Pinson and G. Kariniotakis, "On-line assessment of prediction risk for wind power production forecasts," *Wind Energy*, vol. 7, no. 2, pp. 119–132, 2004.
- [19] E. Holmgren, N. Sibert, and G. Kariniotakis, "Wind power prediction risk indices based on numerical weather prediction ensembles," in *Proceedings of the European Wind Energy Conference*, Warsaw, Poland, 2010.
- [20] J. TASTU, P. Pinson, E. Kotwa, H. Madsen, and H. A. Nielsen, "Spatio-temporal analysis and modeling of short-term wind power forecast errors," *Wind Energy*, vol. 14, no. 1, pp. 43–60, 2011.
- [21] K. C. Sharma, P. Jain, and R. Bhakar, "Wind power scenario generation and reduction in stochastic programming framework," *Electric Power Components and Systems*, vol. 41, no. 3, pp. 271–285, 2013.
- [22] J. B. Bremnes, "Probabilistic wind power forecasts using local quantile regression," *Wind Energy*, vol. 7, no. 1, pp. 47–54, 2004.
- [23] J. B. Bremnes, "A comparison of a few statistical models for making quantile wind power forecasts," *Wind Energy*, vol. 9, no. 1–2, pp. 3–11, 2006.
- [24] R. J. Bessa, V. Miranda, A. Botterud, Z. Zhou, and J. Wang, "Time-adaptive quantile-copula for wind power probabilistic forecasting," *Renewable Energy*, vol. 40, no. 1, pp. 29–39, 2012.
- [25] G. Wang, R. Jia, J. Liu, and H. Zhang, "A hybrid wind power forecasting approach based on Bayesian model averaging and ensemble learning," *Renewable Energy*, vol. 145, pp. 2426–2434, 2020.
- [26] W. Xie, P. Zhang, R. Chen, and Z. Zhou, "A nonparametric Bayesian framework for short-term wind power probabilistic forecast," *IEEE Transactions on Power Systems*, vol. 34, 2019.
- [27] C. Wan, Z. Xu, P. Pinson, Z. Y. Dongg, and K. P. Wong, "Optimal prediction intervals of wind power generation," *IEEE Transactions on Power Systems*, vol. 29, no. 3, pp. 1166–1174, 2014.
- [28] S. D. Kwon, "Uncertainty analysis of wind energy potential assessment," *Applied Energy*, vol. 87, no. 3, pp. 856–865, 2010.
- [29] G. Mokryani and P. Siano, "Evaluating the integration of wind power into distribution networks by using Monte Carlo simulation," *Electrical Power and Energy Systems*, vol. 53, pp. 244–255, 2013.
- [30] X. Zhao, C. Ge, F. Ji, and Y. Liu, "Monte Carlo method and quantile regression for uncertainty analysis of wind power

- forecasting based on Chaos-LS-SVM,” *International Journal of Control, Automation and Systems*, vol. 19, no. 11, pp. 3731–3740, 2021.
- [31] A. Bracale and P. D. Falco, “An advanced Bayesian method for short-term probabilistic forecasting of the generation of wind power,” *Energies*, vol. 8, no. 9, pp. 10293–10314, 2015.
- [32] S. Jung, O. A. Vanli, and S. D. Kwon, “Wind energy potential assessment considering the uncertainties due to limited data,” *Applied Energy*, vol. 102, pp. 1492–1503, 2013.
- [33] C. Gallego, P. Pinson, H. Madsen, A. Costa, and A. Cuerva, “Influence of local wind speed and direction on wind power dynamics-application to offshore very short-term forecasting,” *Applied Energy*, vol. 88, no. 11, pp. 4087–4096, 2011.
- [34] T. S. Nielsen, *Online prediction and control in nonlinear stochastic systems, [Ph.D. thesis]*, IMM, Informatik og Matematisk Modellering, Danmarks Tekniske Universitet, Lyngby, Denmark, 2002.
- [35] G. Sideratos and N. D. Hatziaargyriou, “Probabilistic wind power forecasting using radial basis function neural networks,” *IEEE Transactions on Power Systems*, vol. 27, no. 4, pp. 1788–1796, 2012.
- [36] P. J. Trombe, P. Pinson, and H. Madsen, “A general probabilistic forecasting framework for offshore wind power fluctuations,” *Energies*, vol. 5, no. 3, pp. 621–657, 2012.
- [37] A. Khosravi, S. Nahavandi, and D. Creighton, “Prediction intervals for short-term wind farm power generation forecasts,” *IEEE Transactions on Power Systems*, vol. 4, no. 3, pp. 602–610, 2013.
- [38] K. Beven and A. Binley, “The future of distributed models: model calibration and uncertainty prediction,” *Hydrological Processes*, vol. 6, no. 3, pp. 279–298, 1992.
- [39] R. S. Blasone, J. A. Vrugt, H. Madsen, D. Rosbjerg, B. A. Robinson, and G. A. Zyvoloski, “Generalized likelihood uncertainty estimation (GLUE) using adaptive Markov chain Monte Carlo sampling,” *Advances in Water Resources*, vol. 31, no. 4, pp. 630–648, 2008.
- [40] X. Jin, C. Y. Xu, Q. Zhang, and V. P. Singh, “Parameter and modeling uncertainty simulated by GLUE and a formal Bayesian method for a conceptual hydrological model,” *Journal of Hydrology*, vol. 383, no. 3-4, pp. 147–155, 2010.
- [41] M. Mirzaei, H. Galavi, M. Faghieh, Y. F. Huang, T. S. Lee, and A. el-Shafie, “Model calibration and uncertainty analysis of runoff in the Zayanderood River basin using generalized likelihood uncertainty estimation (GLUE) method,” *Journal of Water Supply*, vol. 62, no. 5, pp. 309–320, 2013.
- [42] G. Aronica, P. D. Bates, and M. S. Horritt, “Assessing the uncertainty in distributed model predictions using observed binary pattern information within GLUE,” *Hydrological Processes*, vol. 16, no. 10, pp. 2001–2016, 2002.
- [43] P. D. Bates, M. S. Horritt, G. Aronica, and K. Beven, “Bayesian updating of flood inundation likelihoods conditioned on flood extent data,” *Hydrological Processes*, vol. 18, no. 17, pp. 3347–3370, 2004.
- [44] N. Sun, B. Hong, and M. Hall, “Assessment of the SWMM model uncertainties within the generalized likelihood uncertainty estimation (GLUE) framework for a high-resolution urban sewershed,” *Hydrological Processes*, vol. 28, pp. 3018–3034, 2014.
- [45] B. Dong, J. Xia, M. Zhou, Q. Li, R. Ahmadian, and R. A. Falconer, “Integrated modeling of 2D urban surface and 1D sewer hydrodynamic processes and flood risk assessment of people and vehicles,” *Science of the Total Environment*, vol. 827, article 154098, 2022.
- [46] A. Montanari, “Large sample behaviors of the generalized likelihood uncertainty estimation (GLUE) in assessing the uncertainty of rainfall-runoff simulations,” *Water Resources Research*, vol. 41, no. 8, article W08406, 2005.
- [47] M. Shafii, B. Tolson, and L. S. Matott, “Addressing subjective decision-making inherent in GLUE-based multi-criteria rainfall-runoff model calibration,” *Journal of Hydrology*, vol. 523, pp. 693–705, 2015.
- [48] F. A. L. Jowder, “Wind power analysis and site matching of wind turbine generators in Kingdom of Bahrain,” *Applied Energy*, vol. 86, no. 4, pp. 538–545, 2009.
- [49] L. Thiaw, G. Sow, S. S. Fall, M. Kasse, E. Sylla, and S. Thioye, “A neural network based approach for wind resource and wind generators production assessment,” *Applied Energy*, vol. 87, no. 5, pp. 1744–1748, 2010.
- [50] T. Burton, D. Sharpe, N. Jenkins, and E. Bossanyi, *Wind Energy Handbook*, John Wiley and Sons, West Sussex, UK, 2001.
- [51] K. Binder and D. W. Heermann, *Monte Carlo Simulation in Statistical Physics*, Springer, Germany, 2010.
- [52] J. E. Nash and J. V. Sutcliffe, “River flow forecasting through conceptual models part I — a discussion of principles,” *Journal of Hydrology*, vol. 10, no. 3, pp. 282–290, 1970.
- [53] C. Y. Chen, *Evaluation of WECS Energy Output by the Generalized Likelihood Uncertainty Estimation Method, [M.S. thesis]*, National Taiwan University, Taipei, Taiwan, 2015.